International Journal of Engineering & Technology, 7 (4.13) (2018) 178-187

International Journal of Engineering & Technology

Website: www.sciencepubco.com/index.php/IJET

Research paper

Simulation framework for civil tiltrotor mission performance

Ezanee Gires*

Department of Aerospace Engineering, Faculty of Engineering, Universiti Putra Malaysia, Malaysia
**Corresponding author E-mail: ezanee@upm.edu.my*

Abstract

A simulation framework for the overall mission performance of a civil tiltrotor system is presented. In this work, a numerical model of a benchmark tiltrotor aircraft's flight dynamics is paired with a high-fidelity simulation of the turboshaft powerplant. The gas turbine simulation of the baseline engine is shown to have high accuracy with its available performance data from flight and stationary tests. The simulation is further validated by the obtained maximum range and endurance performance based on the XV-15 tiltrotor. The power requirements during the different phases of tiltrotor flight are also modelled including the transition phases between rotary- to fixed-wing. A mission framework is designed to show the estimated fuel burn and emissions. The mission procedures are based on the flight envelope data available in the public domain as well as modern helicopter operations. This work can be used as the baseline for the modelling of conceptual configurations of civil tiltrotors, particularly for variations in powerplant technologies.

Keywords: *gas turbine engines; mission performance; rotorcraft simulation; programming and simulation; tiltrotors.*

1. Introduction

The conventional helicopter with single main- and tail-rotor is used in diverse operations requiring high manoeuvrability and stability in low speed flight and hover. The main rotor, however, is limited in high speeds in the region of 200 kt [1]. Thus, in order to have both high speed flight and also vertical takeoff and landing (VTOL), an aerodynamic lifting surface or vectored thrust needs to be incorporated into the rotorcraft paradigm [2]. Figure 1 shows the lift/hover power and speed capabilities of various VTOL concepts against disk loading.

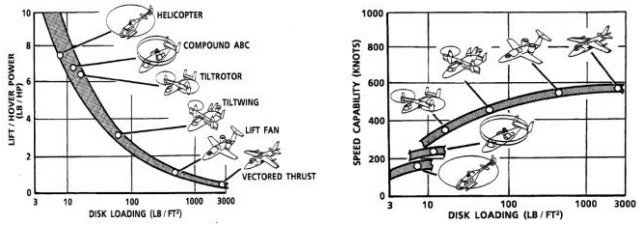

(a) (b)

Fig. 1: (a) Hover and (b) Speed capability of VTOL concepts [3]

Lift/hover power is a reflection of a VTOL aircraft's compromise between efficient hover and high speed cruise [1]. For the tiltrotor, the main contributors for lift are the twin, counter-rotating main rotors in hover and low-speed forward helicopter flight, while the fixed-wing provides increasing lift with progressive forward speeds. Tiltrotors have greatly expanded range and speed over the conventional helicopter. In helicopter flight, power requirements (and fuel burn) are comparable to helicopters because of the side-by-side proprotors which expand the overall lift span [4].

Civil tiltrotors (CTR) such as Leonardo (formerly Agusta-Westland) AW609 will play a pivotal role in reducing airport congestion and intercity and megalopolitan transportation bottlenecks, relieving air transportation gridlock and airport capacity saturation [5,6]. As shown in Figure 2, integration of a CTR system into the airspace could reduce the time between start- and end-points compared to comparably-sized fixed-wings.

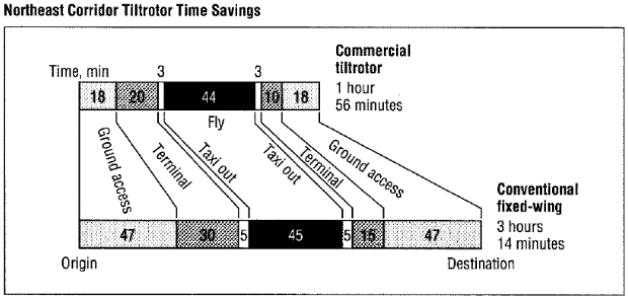

Fig. 2: CTR time savings compared to conventional fixed-wings [7]

According to Dreier [8], a tiltrotor simulation program must be able to perform simple trim calculations and be able to calculate stability and control derivatives and execute general equations of motion in the time domain. A simulation program would consist of modules with the ability to calculate, from empirical models or data tables, the requisite forces or power requirements in a given timestep. These would include the powerplants, transmission, main rotors, airframe, controls and atmospheric or ambient conditions. From Padfield [9], the integration of a rotorcraft simulation model into a mission performance framework would have a flight task hierarchy that begins with operation or mission design, mission task elements, and ends with individual manoeuvre calculations.

Prior to the NASA Heavy Lift Rotorcraft Systems Investigation initiated in 2005, computational tools for the design and analysis of rotorcraft used low-fidelity models for rapid convergence [10]. In the late 2000s, Johnson, Datta and Russell [11,12] identified the requirements for the next generation comprehensive analysis of rotorcraft. Johnson and Datta [11] pointed out that first generation (legacy) tools are limited by design, as they were restricted to

specific rotorcraft configurations and rotor types. The NASA Design and Analysis of Rotorcraft (NDARC) framework was created in response [10]. Russell and Johnson [12] used NDARC to generate a Large Civil Tiltrotor (LCTR) design based on climate metrics.

Fixed-wing studies mainly use simplified L/D models of aircraft and looked at discretised mission segments rather than a time-history analysis of fuel burn trends. Thus, a preliminary tiltrotor mission performance framework, linking the airframe to validated and conceptual powerplants, is developed and validated. This also fills the gap in tiltrotor simulation, where most academic studies have been purely focused on modelling dynamics and control rather than a mission-based approach to obtain CTR fuel burn and emissions.

2. Tiltrotor simulation model

The primary task is to establish a framework for total mission fuel burn calculation. With this information, the gross takeoff weight (GTOW) and overall emissions for a given powerplant and mission profile can be ascertained. Filippone [13] lays out a general procedure which involves calculating the fuel required for each mission segment and updating the GTOW, iterating until the error between the initial GTOW guess and final GTOW is sufficiently reduced. Newman [14] goes into a bit more detail with regard to mission fuel calculations, but uses average speeds only for each leg. No acceleration is considered and fuel flow is calculated using simplified engine coefficients. It was clear that greater fidelity was required in order to properly estimate the performance of the civil tiltrotor (CTR) across a detailed mission profile divided across many timesteps. As such, the author followed the example of Goulos [15] who employed a multidisciplinary approach incorporating advanced rotor inflow modelling as well as linking the aeromechanical code with Cranfield University's in-house Turbomatch engine simulation program.

The mathematical model used to calculate the aero-loads and power requirements of the civil tiltrotor is based on the NASA Generic Tilt-Rotor Simulation (GTRSIM) program initially developed by Harendra *et al.* [16] and later updated by Ferguson [17]. The analogues used to model the tiltrotors at the time were the Bell Model 301 followed by the Bell XV-15. Despite the specificity of the benchmark tiltrotor used by the mathematical model, many of the coefficients and lift and drag tables can be swapped out for other models, allowing for a generic tiltrotor simulation model. Additional calculations in terms of engine installation weight and airframe-engine coupling (fuel flow) are linked to the aeromechanical model and are new additions to the existing GTRSIM algorithm. Trim calculation, mission-specific calculations and fuel burn estimation are features that were not in the original GTRSIM program. The author adapted the mathematical formulae and procedures to modern Fortran to produce a tiltrotor mission performance simulation framework. A flowchart summarising the various processes of the created CTR program is shown in Figure 6. Further derivation and explanation of the components' calculations can be found in Ref. [18].

2.1. Tiltrotor aeromechanics and trim

In a multidisciplinary program, the aircraft must be brought to trim before calling the powerplant simulation module. For a rotorcraft, this means that the control inputs must be iteratively updated to bring the total body forces and moments to zero. For the CTR framework mentioned here, longitudinal trim is prioritised to reduce complexity. Additionally, lifting surface controls (wing and empennage flaps and flaperons) are scheduled based on pylon tilt angle and forward speed, while fuselage angle is a function of published XV-15 data [19] and gross weight (GW). The chosen baseline model for the development of the tiltrotor framework presented here is the XV-15 due to the wealth of data available in the public domain. Some pertinent data relevant to geometry is presented in Table 1. The Bell XV-15 is depicted in Figure 3.

Fig. 3: Bell XV-15 [15]

Table 1: Selected XV-15 data

Description	Symbol	Value	Units
Design gross weight	DGW	13,000.0	lb
Number of blades	n_b	3	-
Radius of rotor disk	R	12.5	ft
Blade chord	c_b	1.167	ft
Rotor speed, $0 \leq \beta_M < 90$	-	589	RPM
Rotor speed, $\beta_M = 90$	-	517	RPM
Wing span	b_W	32.17	ft
Wing chord	c_W	5.225	ft
Wing sweep at quarter-chord	$(\wedge_{c/4})_W$	-6.5	Deg
Horizontal stabilizer area	S_H	50.25	ft^2
Vertical stabilizer area	S_V	50.5	ft^2

In all cases where the forces and moments of the above components are calculated, the influence of the induced velocity of the rotor (downwash or rotor wake) is included. This particularly applies to the helicopter configuration flight segments, where the effect of rotor wake on the wing-pylon surface is most keenly felt. In the mathematical model, the forces and moments are calculated first in their local wind axes, and then rotated to body forces in relation to the aircraft centre of gravity, CG. These forces and moments are then totalled together to form the aircraft equations of motion. The body axis velocities and accelerations, both linear and angular are converted from wind to body axes by means of Euler angles [8,15].

An important control parameter in tiltrotor analysis is the mast (pylon) tilt angle β_M. The author has chosen to assume that the default pylon setting is in the upright (helicopter) position ($\beta_M = 0°$), and the tilt of the mast is in the horizontal forward direction up to $\beta_M = 90°$ (airplane). This is shown in Figure 4.

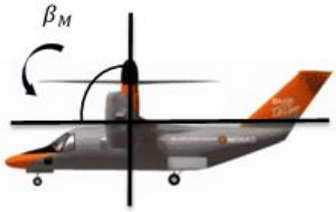

Fig. 4: Direction of mast tilt

Figure 5 encapsulates the processes involved in performance calculations and trim for each timestep in a mission leg while Figure 6 shows the CTR mission simulation workflow.

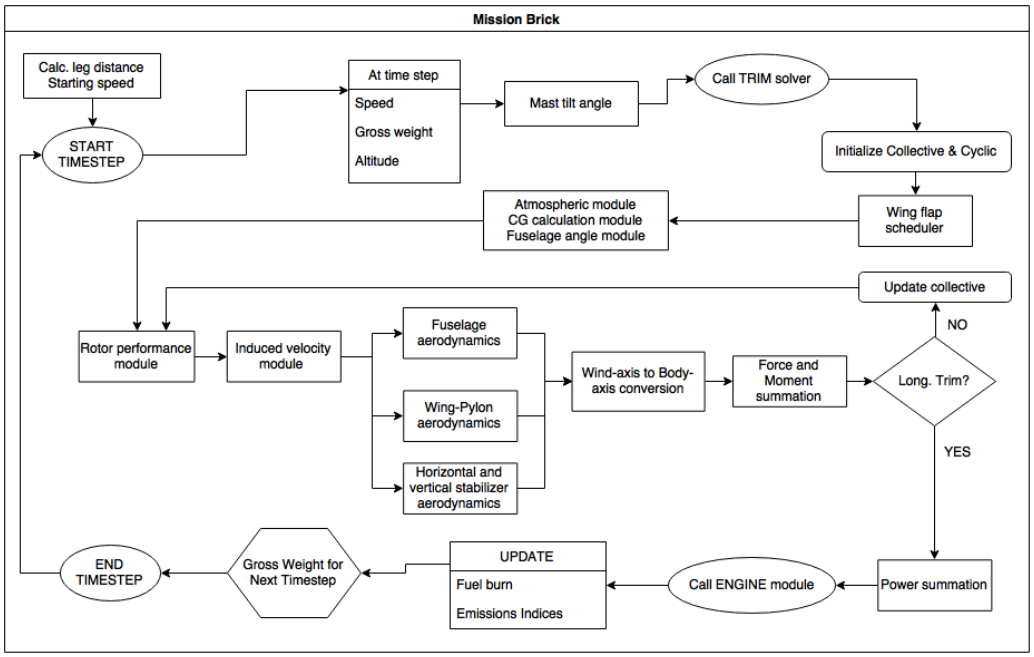

Fig. 5: CTR trim procedure to update gross weight at each timestep

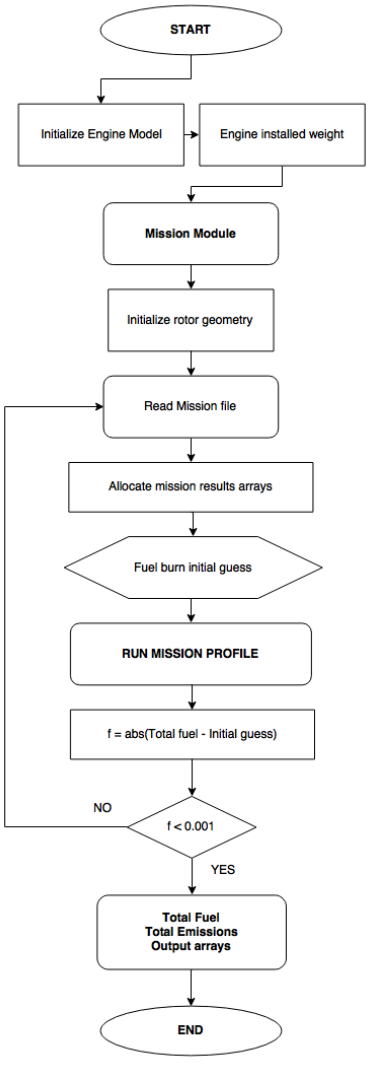

Fig. 6: CTR mission simulation workflow

2.2. Rotor aerodynamics

The assumptions for rotor calculations are as follow:

1. Average values for lift-curve slope and profile-drag coefficient are used over the entire span of the blade and are adjusted to approximate rotor thrust and power required characteristics.
2. Blade angle of attack α_r is approximated by $\sin(\alpha_r)$. This substitution in the blade element equations enables the calculations for rotor forces without restricting blade pitch θ and inflow angle ϕ to small angles.
3. Blade flapping with respect to the mast is considered to be small (small angle assumption); harmonics of flapping above 1/rev are ignored.
4. Blade flapping equations assume the rotor is in equilibrium condition (to reduce complexity)

Rotor induced velocity, v_i is computed by calculating the induced velocity of the isolated out of ground effect (OGE) rotor and by modifying the induced velocity to account for a side-by-side rotor effect and OGE operation. This is given in Eqn. 1, where C is defined as $C = C_T/2B^2$. The 0.866 factor on λ^2 is added to improve power correlation in hover.

$$v_i = \frac{(\Omega R)C}{\sqrt{0.866\lambda^2 + \mu^2} + \frac{0.6|C_T|^{1.5}\left(|C_T| - \frac{8}{3\lambda}|\lambda|\right)}{(|C|+8\mu^2)(|C|+8\lambda^2)}} \quad (1)$$

Among the coefficients calculated is the blade lift coefficient corresponding to the advance ratio and mast tilt as in Eqn. 2, where a_0, a_1, a_2 are blade lift coefficients.

$$a_R = a_0 + \mu_R(a_1 - a_2\mu_R) \quad (2)$$

Ferguson updated Eqn. 2 to include the blade tip Mach number as shown in Eqn. 3.

$$a_R = [a_0 + \mu_R(a_1 - a_2\mu_R)]\left(\frac{1}{\left[1 - (0.75M_{tip})^2 \sin\beta_M\right]^{\frac{1}{2}}}\right) \quad (3)$$

The recommended generic (from the XV-15) values for blade lift coefficients are $a_0 = 4.95$, $a_1 = 8.0$, and $a_2 = 30$. The rotor cyclic longitudinal input $\bar{B}_{1R/L}$, is calculated in every update cycle. Lateral cyclic is 0, since tiltrotors only use longitudinal cyclic (as both counter-rotating rotors cancel each other's torque).

The calculation of induced velocity and thrust in helicopter forward flight involves an iterative solution. The induced velocity is a function of the rotor thrust, forward speed and vertical speed; however, rotor thrust by itself is a function of induced velocity [8, 13]. In the early performance analysis of the tiltrotor, the author used the Newton—Raphson method to solve for induced velocity for the isolated rotor, as demonstrated by Filippone [13]. The results from this method are rotor thrust $T_{R/L}$, thrust coefficient $C_{T_{R/L}}$, and induced velocity $W_{iR/L}$.

The main purpose of calculating the rotor characteristics is to determine the rotor power required in addition to the rotor torque required (positive indicating the torque required to slow the rotor down [16]). This is especially necessary in order to match rotor power with engine power. The general equation of rotor power required is given by Eqn. 4 [13], which is a combination of induced power, profile power, and parasitic drag power. Additional drag power is obtained from the aerodynamics of the other lifting surfaces of the CTR.

$$P_{req} = P_i + P_0 + P_p \tag{4}$$

The rotor wake is assumed to affect the wing lift and drag, the horizontal stabiliser and vertical fin (empennage) lift and drag, and the rotor wake-airframe-ground interaction in producing a net rolling moment and pitching moment effects when hovering near the ground. The rotor wake effect on the fuselage is considered negligible due to placement of the proprotors away from the fuselage.

The calculation of wing aerodynamic forces and moments due to rotor wake effects is made separately from the forces and moments generated by freestream flow. The rotor wake is assumed to affect the portion of the wing directly below the rotors. This area on each wing is designated S_{iW} and is computed as a function of wake radius, conversion angle, wake angle of attack, and sideslip angle of the fuselage. For the each rotor, the rotor wake ratio R_{WR} (subscript R indicating right proprotor) is calculated as (XV-15) can be calculated using Eqn. 5.

$$R_{WR} = R\{0.78 + 0.22\exp[-(0.3 + 2Z\sqrt{C_{RFR}} + 60C_{RFR})]\} \tag{5}$$

The Z component of Eqn. 5 is the ratio of mast length l_M and rotor radius R. C_{RFR} refers to the right rotor thrust coefficient, as calculated using Eqn. 6.

$$C_{RFR} = \frac{\sqrt{T_R^2 + H_R^2 + Y_R^2}}{\rho\pi\Omega_R'^2 R^4} \tag{6}$$

The rotor wake effects on the wing, horizontal and vertical stabilizers are either washed out or maximised depending on mast angle β_M; for the helicopter configuration, $\beta_M = 0°$ and so the rotor wake only acts in the *W*-directional component, while for the airplane configuration, $\beta_M = 90°$ and so the rotor wake only acts in the *U*-directional component.

2.3. Wing, empennage and fuselage

For the fuselage, wing and stabilisers, lift and drag coefficients are obtained from literature (wind-tunnel or flight test data) [1,16,17]. Forces and moments are thus numerically calculated in their respective modules and updated with every iteration of rotor induced velocity until convergence of trim. For the XV-15, wing-pylon lift and drag coefficients are provided for mast angles of 0 and 90 degrees and for 4 flap settings. The coefficients for intermediate mast angles and flap settings are obtained by interpolation. XV-15 aerodynamic coefficients for angles of attack up to stall are based on wind tunnel data. The angle of attack of the wing is modified to reflect the induction effect of the thrusting rotors as given by Eqn. 7.

$$\alpha_W = \alpha_F - \left(0.26x_{R/W}\frac{2C_{RF}}{MAX^2(\mu, 0.15)}\frac{180}{\pi}\right) \tag{7}$$

α_W is the angle of attack on the portion of the wing outside the rotor wake. α_F is the fuselage angle of attack. $x_{R/W}$ is the induction coefficient and is a function of the distance between the rotor and wing, and C_{RF} is the non-dimensionalized rotor force coefficient. The values for pylon interference drag are corrections or additions to the original mathematical model to account for extra drag due to wing-pylon interference. The effect of pylon drag is significant in the deceleration of the tiltrotor during reconversion to helicopter mode [17]. Since the formulation of spinner drag is available in the literature [21], the author has included it in the overall contribution to total aircraft forces. Furthermore, Johnson states that tiltrotors typically use spinners as opposed to conventional helicopter hubs due to the proprotor conversion to airplane mode [21].

Up to one third of the XV-15's mass comprises of its nacelles (including engines and transmission) [1]. During transitional flight, the vehicle's centre of gravity (CG) shifts due to pylon tilt. In order to predict the vehicle behaviour, the CG and inertia shift with pylon tilt need to be calculated. The datum point for the CG shift is the CG of the helicopter configuration in terms of station line and water line ($\beta_M = 0°$). Eqn. 8 and Eqn. 9 represent the CG displacement as a function of the pylon tilt angle, where $X = \frac{W_P}{GW}\frac{(SL_{SP}-SL_P)}{12}$ and $Z = \frac{W_P}{GW}\frac{(WL_{SP}-WL_P)}{12}$ (if using inches and feet as units of measure). W_P is the combined pylon weight and GW is the gross weight of the tiltrotor.

$$X_{CG} = Z\sin(\beta_M) + X(1 - \cos\beta_M) \tag{8}$$

$$Z_{CG} = Z(1 - \cos\beta_M) - X(\sin\beta_M) \tag{9}$$

The updated CG location is then given by Eqn. 10 and Eqn. 11.

$$SL_{CG} = SL_{CG}|_{\beta_M=0} + (X_{CG}) \tag{10}$$

$$WL_{CG} = WL_{CG}|_{\beta_M=0} + (Z_{CG}) \tag{11}$$

The calculation of rotor hub height from ground (here in unit ft) is given by Eqn. 12.

$$h_H = h_{CG} + \left\{l_M\cos\beta_M + \frac{WL_{SP} - WL_{CG}}{12}\right\} \tag{12}$$

2.4. Summation of forces and moments

The general form of transformation from body to wind axis is as shown in Eqn. 13.

$$\begin{bmatrix} X_i \\ Y_i \\ Z_i \end{bmatrix}_{body} = \begin{bmatrix} \cos\alpha_i\cos\beta_i & -\cos\alpha_i\sin\beta_i & -\sin\alpha_i \\ \sin\beta_i & \cos\beta_i & 0 \\ \sin\alpha_i\cos\beta_i & -\sin\alpha_i\sin\beta_i & \cos\alpha_i \end{bmatrix}\begin{bmatrix} X_i \\ -Y_i \\ Z_i \end{bmatrix}_{wind} \tag{13}$$

The terms α_i and β_i refer to the angle of attack and sideslip of the component in question. Here, sideslip is zero to reduce complexity. The trim calculation as shown in the flowchart in Figure 5is contingent on zeroing the total Z-forces and pitching moments. For each timestep, the control inputs to be iterated are the collective and cyclic pitch. However, in order to reduce computational load and time, the priority was on ensuring the collective pitch error was more quickly reduced. To that end, fuselage pitch is scheduled based on GW, speed, altitude and mast tilt angle and the flaps are scheduled on tilt angle and speed.

3. Powerplant modelling

The performance of the baseline and conceptual powerplants at design point (DP) and off-design (OD) is calculated using the in-house Cranfield gas turbine simulation program Turbomatch [22]. The DP and OD calculation is performed through iterations using generic component maps. Turbomatch engine models are comprised of discrete bricks designating the function of each component. The baseline engine is the Lycoming LTC1K-4K, a variant of the T53-L series installed in the Bell XV-15. The DP performance of the Turbomatch model is matched with the published Lycoming data in terms of mass flow and specific fuel consumption at maximum takeoff power (1550 SHP). The schematic of the baseline engine is shown in Figure 7. The design parameters and DP performance of the Turbomatch model is compared to the data from Jane's Aero Engines [23] in Table 2.

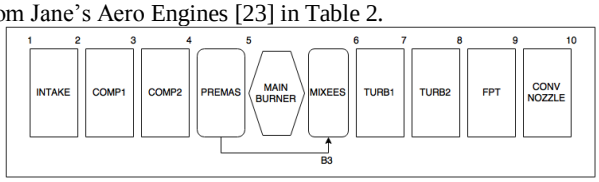

Fig. 7: Baseline engine Turbomatch schematic

Table 2: Lycoming LTC1K-4K engine model design parameters

Design parameter	Unit	Value	Turbomatch value	Error (%)
Max takeoff power (DP)	HP	1550	1550	-
Inlet mass flow	kg/s	4.85	4.85	0.00
Specific fuel consumption	μg/J	98.70	99.72	1.03
Overall pressure ratio	-	7.05		-
Turbine entry temperature	K	1450		-

The DP performance of the baseline engine matches well with the measured data for the LTC1K-4K. While the engine model is not exactly the same, some fuel flow data is available for the Lycoming T53-L-13 from Rubins and Doyle [24]. The maximum power difference for the T53 engine is approximately 100 SHP less than that of the LTC1K-4K. The trends are compared for the baseline engine OD points and the 1973 report below in Figure 8. It is shown that the trends compare well albeit with slightly higher fuel flow for the baseline.

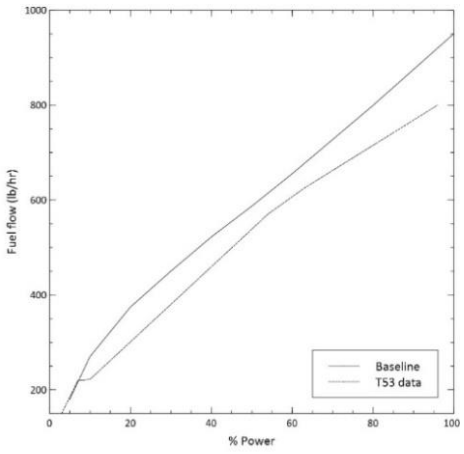

Fig. 8: Baseline engine against T53-L-13 fuel flow trends

The engine model fuel flow at various tilt angles and airspeeds is compared against measured fuel flow from XV-15 benchmark data at standard sea level conditions and DGW [25]. This is shown in Figure 9. The CTR program tends to agree with the benchmark data particularly at high speeds for each mast tilt angle; meanwhile, some errors are noticeable at low speeds, but are small in magnitude and the trends of both lines are similar. While the program power curves for the AP configuration at altitudes higher than sea level better match the published power curves at 12000 and 20000 ft, no available measured fuel flow data is available for comparison. Moreover, much of the time spent in AP mode is at higher altitudes where the Turbomatch fuel burn should closely approximate actual fuel burn values.

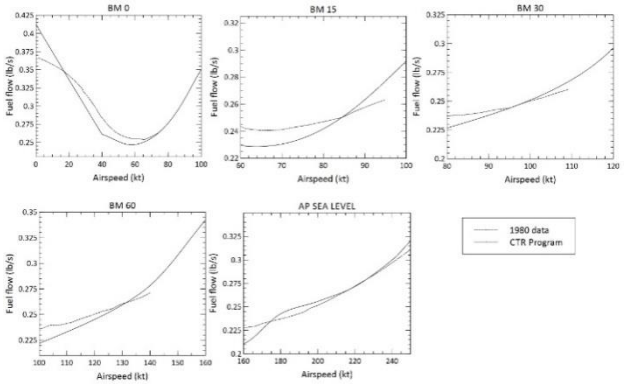

Fig. 9: Benchmark fuel flows vs simulation fuel flow at sea level

3.1. Calculation of emissions

The NO_x, unburned hydrocarbon (HC), CO, and particulate matter (PM) emissions are calculated by means of emission indices (EI) from the Swiss Federal Office of Civil Aviation (FOCA) [26]. These values are from measured emissions of helicopter turboshaft engines of varying power classes. For this research the EI values are for engines of power 1000 SHP and above. The same correlation was used for validation by Ali [27] and Zhang [28]. The EI for NO_x, HC, CO and PM are based on the turboshaft engines of power above 1000 SHP, given by Eqn. 14 to Eqn. 17, respectively. The EI for CO_2 is a linear 3.16 kg CO_2 for every kg of fuel burnt [12].

$$\text{EI } NO_x(\text{ g/kg fuel }) = 0.2113 \times (\text{SHP})^{0.5677} \quad (14)$$

$$\text{EI HC}(\text{ g/kg fuel }) = 3819 \times (\text{SHP})^{-1.0801} \quad (15)$$

$$\text{EI CO}(\text{ g/kg fuel}) = 5660 \times (\text{SHP})^{-1.11} \quad (16)$$

$$\text{EI PM}(\text{g/kg fuel}) = -4.8 \times 10^{-8} \times \text{SHP}^2 + 2.3664 \times 10^{-4} \times \text{SHP} + 0.1056 \quad (17)$$

The EI above are verified against FOCA tables (NO_x) and validated with the T53/55 emissions report from Rubins and Doyle [24] for NO_x and CO in Figure 10.

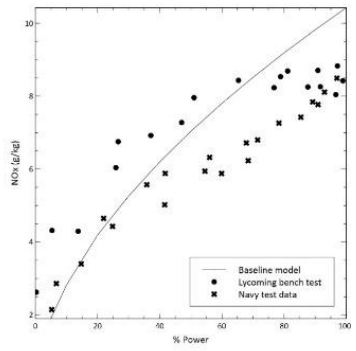

(a)

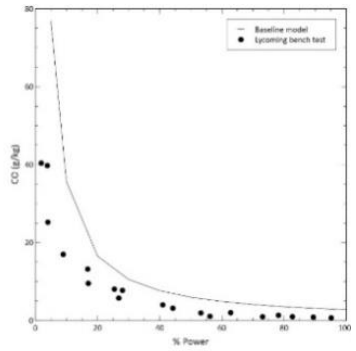

(b)

Fig. 10: NO_x and CO emissions validation against T53 data

The FOCA turboshafts referred to in the legend for Figure 11 are unfortunately not specified in the FOCA manual [26] beyond the numbering convention showed; however, it is understood that the different datasets represent different shaft horsepower outputs from their database. Therefore, it is assumed that Data 3 and 4 represent the upper bound of the EI formula, while Data 1 and 2 represent the lower bound. The NO_x calculated emissions for the baseline engine match well with the T53 data and are within the upper and lower bounds of the FOCA database.

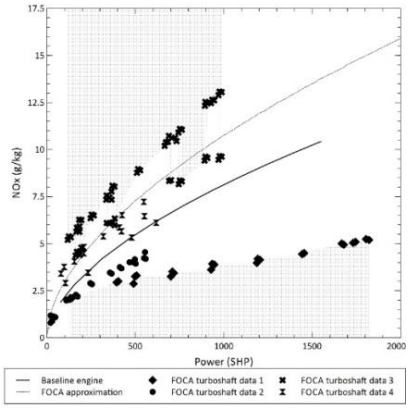

Fig. 11: FOCA NOx validation

4. Validation of CTR model

The combined CTR code is validated against several publications featuring other mathematical models, simulations, wind tunnel measurements and flight test data for the XV-15. The validation parameters shown here are power required per engine at various mast tilt angles. More validation data can be found in [18]. The mathematical model data is from the Harendra *et al.* code from 1980 as obtained by Churchill and Dugan [29]; the same source provides wind tunnel data from 1978. Simulation via the NASA Design and Analysis of Rotorcraft tool (NDARC) and flight data is obtained from Johnson [30]. Validation of the rotor thrust from trim is based on thrust calculated by the GTRSIM program [31]. GTRSIM data is referred to in the legends as 1989 mathematical model data. For Figure 12(a) – (d), the standard error is indicated with respect to the mean of available validation data.

Padfield [9] lists three levels of mathematical modelling of rotors and thus three levels of simulation. With regard to the complexity of the rotor mathematical model employed, the model falls firmly within Level 1; the qualification being simpler aerodynamic modelling as well as rigid blade assumptions. Levels 2 and 3, which include aeroelastic and nonlinear inflow analysis, would certainly improve the fidelity but are considered superfluous for this stage. While the standard error for airplane mode at sea level increases with forward speed, there is agreement with flight test data and high-speed airplane flight above 200 kt is limited to higher cruise altitudes.

5. Design of mission performance framework

The majority of time spent in flight for a tiltrotor is in fixed wing cruise. However, a properly designed mission complete with procedures for takeoff, landing and conversion from helicopter (HC) to airplane (AP) and reconversion from AP to HC is important to fully capture the fuel burn trends across the entire mission profile. The procedures for various CTR flight segments are described below and serve to approximate the expected procedures for an actual CTR mission, since tiltrotors have not yet been put into active service in the civil airspace. The mast tilt angle during conversion is based on design and flight data of the XV-15. Wernicke and Magee [32] provide a useful guide on the conversion corridor and the flight test data is reproduced below in Figure 13.

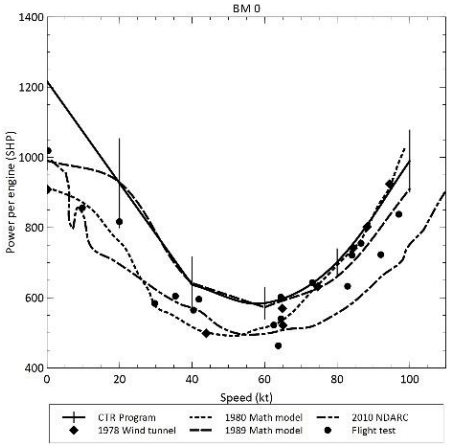

(a) $\beta_M = 0$

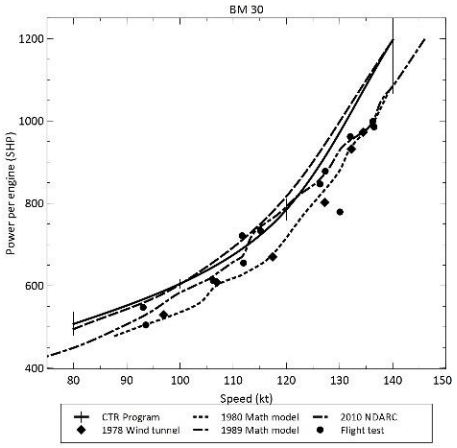

(b) $\beta_M = 30$

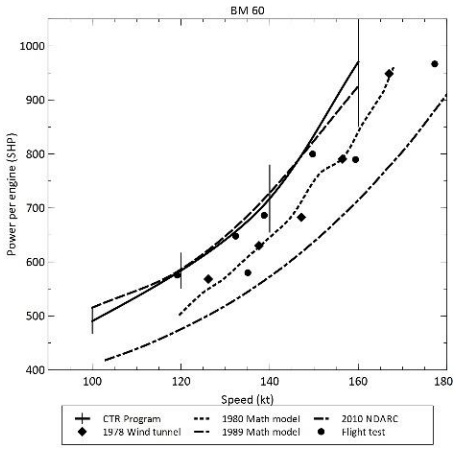

(c) β_M = 60

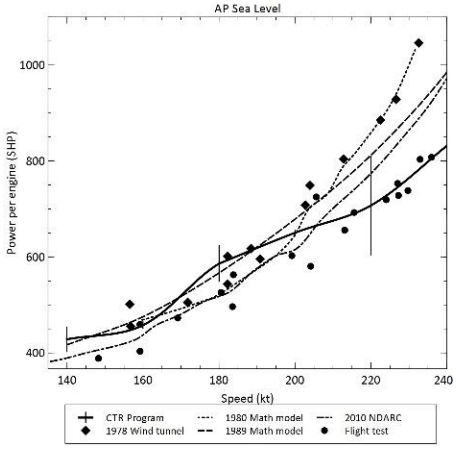

(d) β_M = 90, SSL

Fig. 12: XV-15 power per engine validation

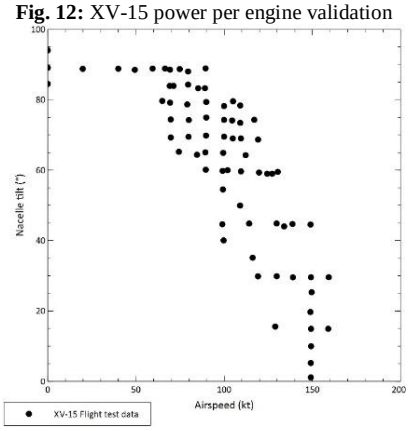

Fig. 13: Conversion corridor for the XV-15 based on flight test data

It is important to note that continuous tilting of the rotor pylons (real-time or transient) is not modelled. Instead, mast angles are set in 15°-30° increments and are based on flight speed. However, during the conversion or reconversion segments, the timestep is reduced from 10-15 s to 1 s so that fuel flow can be calculated in finer increments. In addition, mast angle can be defined by the user in the mission files read by the tiltrotor performance program.

5.1. Takeoff and conversion from helicopter to airplane mode and reconversion for landing

Tiltrotors are designed for vertical and short takeoff and landing (V/STOL). In order to standardise the takeoff procedure for this research, only takeoff in helicopter mode (β_M 0°) is considered. The takeoff to climb procedure is adapted from the XV-15 Familiarization Document [33]. Prior to takeoff, both engines are set to idle at 20% maximum torque each for 5 minutes. Then, hover is initiated for 2 minutes followed by level acceleration to 30 kt. The CTR then climbs to 2000 ft above ground level (AGL) to 60 kt HC, proceeding to conversion to AP at level altitude and accelerating to 200 kt. In HC – AP conversion, the mast tilt angle is scheduled based on forward airspeed and the aforementioned conversion corridor. β_M is set to 15° when the forward airspeed exceeds 60 kt, 30° at 80 kt, 60° at 100 kt and 90° (AP) at or above 140 kt. The rate of acceleration during conversion is modelled as 0.4 g. Upon reaching 200 kt at 2000 ft AGL, the CTR climbs to cruise altitude at a fixed ROC of 2400 ft/min.

The reconversion from AP to HC occurs just before the landing approach. The CTR first descends from cruise altitude to the approach altitude to be used in HC flight. To incorporate a plausible descent profile, the rate of descent (ROD) chosen in the mission design is based on the Beechcraft Super King Air B200 turboprop, which has a similar DGW and size to the XV-15. In this case, the ROD is 1500 ft/min based on the Pilot's Operating Handbook for the B200 [34]. The CTR continues to decelerate to 60 kt at level altitude with scheduled changes in β_M from 90° to 0° depending on airspeed. β_M is set to 60° when the forward airspeed hits 140 kt, 30° at 100 kt, 15° at 80 kt and 0° at or below 60 kt. During the reconversion from AP to HC the rate of deceleration is 0.06 g to simulate the braking effect from tilting the nacelles upward, based on Conner *et al*. [35].

The CTR landing approach is based on approach profiles detailed by Conner *et al*. in their practical research on XV-15 low noise approaches. Upon reaching the LP, the CTR is brought to hover in ground effect (IGE) before setting down and idling for 1 minute. Although noise is not modelled here, it was reported by Conner *et al*. that this approach was close to Federal Aviation Authority (FAA) noise certifications for conventional helicopters.

5.2. Mission performance incorporation into CTR code

The CTR of weight class 6000 kg (~13000 lb) such as the XV-15 or its successor the AW609 is expected to perform a variety of missions that take advantage of its manoeuvrability, range and speed. To demonstrate the versatility of the medium class CTR, Figure 14 shows the variety of cabin layouts for the AW609 to suit different mission types.

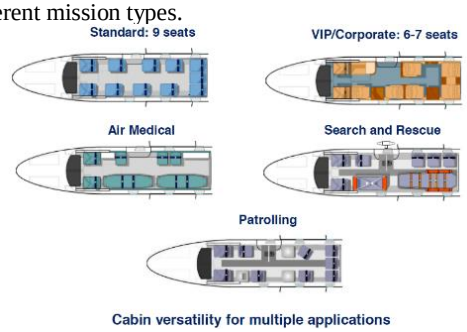

Fig. 14: AW609 cabin layouts [36]

The mission module is designed to read from the mission input file discrete bricks and relevant starting information. The mission input file is adapted from the Helicopter Omni-disciplinary Research platform (HECTOR) format developed and established by Goulos [15]. In order to simplify the process, nine bricks are defined to be read by the CTR program which can be modified depending on the mission requirements. These bricks are outlined in Table 3. The maximum range of the CTR modelled is validated against the ostensible maximum range of the XV-15. Hover endurance of the model in helicopter mode is also modelled and validated. These payload-range and hover endurance plots are shown in Figure 15.

Table 3: CTR mission bricks

Brick	Description	Details
Data_Start	Initial Data Relevant To Mission	Initial Guess For Total Fuel Burn Mission Time Guess
Mission_Start	Initial Location	Starting Coordinates Mission Ground Altitude
Idle	Engine Idle	Engine Torque Fraction
Payload	Pilots, Passengers, Luggage Or Equip-ment Weight	Delta Mass (Loading/ Offloading)
Hover	Hover In HC Mode	Duration Altitude
Cruise_HC	Flight In HC Mode Or $\beta_M < 90°$	Start/End Coordinates, Altitude, Speed Climb Rate
Conversion_AP	Conversion To AP Mode (Level Flight Only)	Start/End Coordinates, Speed
Cruise_AP	Flight In AP Mode (β_M 90°)	Start/End Coordinates, Altitude, Speed Climb Rate
Conversion_HC	Conversion To HC Mode (Level Flight Only)	Start/End Coordinates, Speed

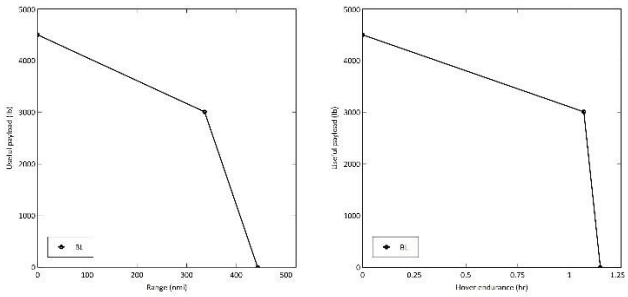

Fig. 15: Maximum range and hover endurance of CTR model

The obtained range of 443 NM is in very good agreement with the official figure of 445 NM. The baseline hover and range performance tallies well with the XV-15 data [33]. With these bricks and

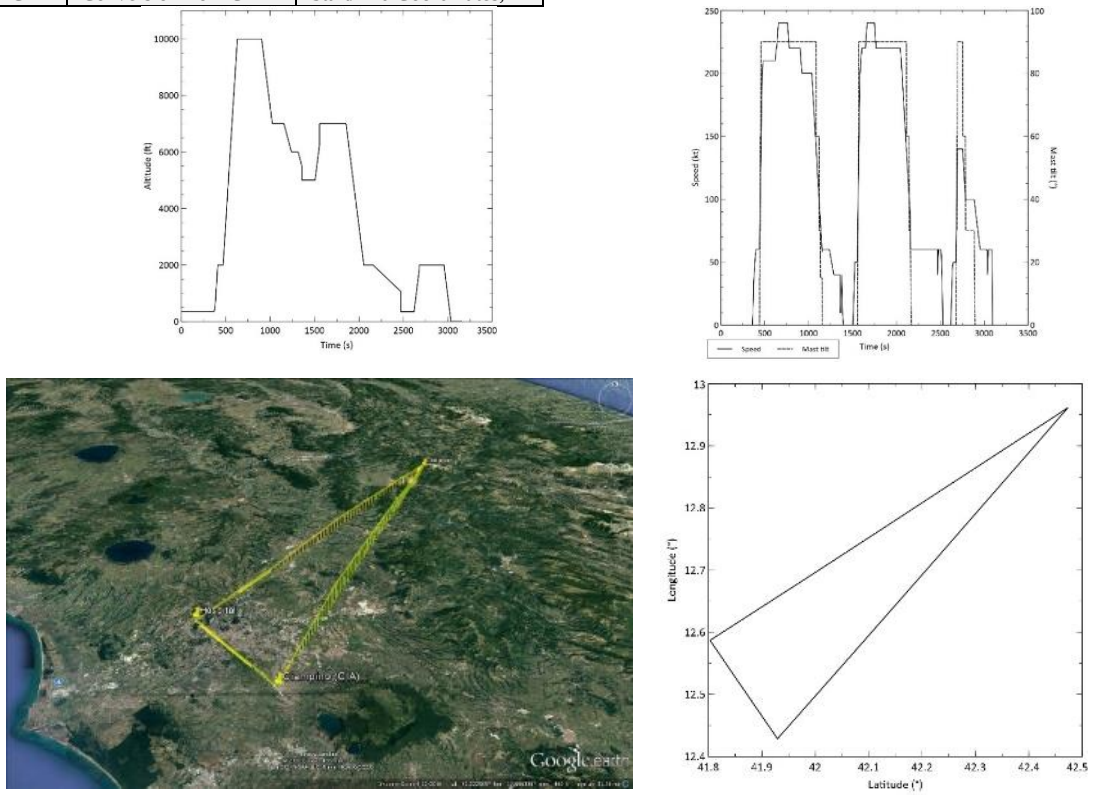

Fig. 16: EMS mission profile

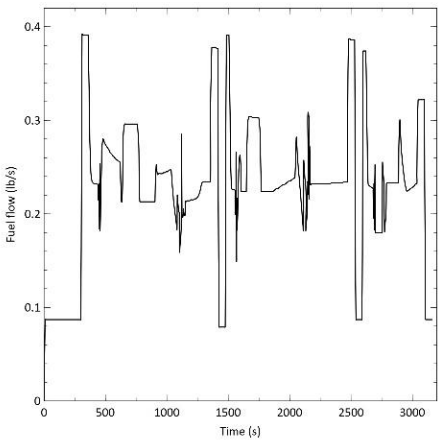

Fig. 17: Fuel flow vs time for EMS scenario

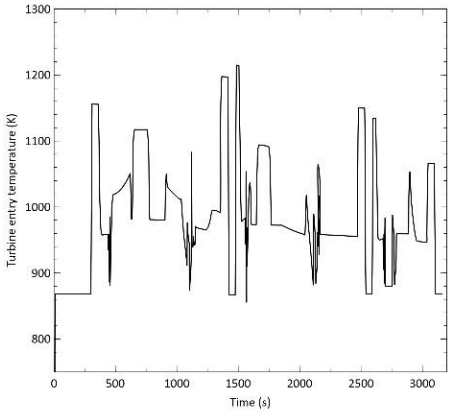

Fig. 18: Turbine entry temperature for EMS scenario

standardised procedures, defining a mission only requires knowing the purpose of the mission, payload, coordinates and maximum cruise height. An example of a mission designed using this method is an Emergency Medical Services (EMS) scenario.The amount of reserve fuel onboard is 10% (149 lb) of fuel tank. The total weight of the two pilots is assumed to be 400 lb. Figure 16 shows the altitude, speed and trajectory profiles for the mission. The fuel burn history and turbine entry temperature (TET) history for the EMS mission are shown in Figures 17 and 18. The mission level results for the baseline presented in Table 4.

The results obtained are useful in identifying the portions of a given flight scenario that require large amounts of fuel flow or power. For engine diagnostics, the time history of turbine entry temperature is particularly important in determining the long-term health of the engine and its maintenance scheduling. In this instance, because the power required did not reach the limitation of ~3000 SHP, the TET did not approach the set limitation of 1450 K. For tiltrotors in particular, it is useful to know the power and fuel requirements in the transitional phases of the flight (conversion / reconversion). While the transients are not available from the numerical model, the results from the time-step analysis can provide a reasonably acceptable value when accounting for total mission fuel burn. The total fuel burn and estimated emissions as shown in Table 4 are based on the baseline Lycoming engines. It is expected that an optimised turboshaft with conventional technology or even technologies such as reheat or heat exchangers would yield improvements in both fuel and environmental impact.

Table 4: EMS mission results for baseline engine

EMS mission (Range 175 km)	
Total time (mins)	52.6
Fuel burn (kg)	321.76
CO_2 (kg)	1095.30
NO_x (kg)	4.50
CO (kg)	1.32
Unburned hydrocarbon (kg)	1.07
Particulate matter (kg)	0.118

6. Conclusion

The development and validation of a generic, rapid code for the simulation of civil tiltrotor has been presented. The primary purpose has been to provide a platform for modular changes to the various components of a tiltrotor aircraft. This is especially important for simulation of powerplants to ascertain the fuel and environmental (emissions) impact of a given mission profile. This can be beneficial in two areas: (i) modelling existing and baseline powerplants for civil operators using a fleet of CTRs; and (ii) modelling conceptual engines that are incorporated into existing airframes. For the latter, this becomes even more relevant in light of increasing calls for high efficiency gas turbines and the emergence of electric engines that are capable of powering manned aircraft.

Acknowledgements

The author wishes to thank Vassilios Pachidis of Cranfield University for his supervision of this project. Further thanks are extended to Konstantinos Karamolegkos, Ioannis Goulos, Fakhre Ali, Evangelos Chrysochoidis, Julien Enconniere, Jesús Carretero, Alejandro Pardo and JinXiu Zhang. This work was supported by the *Malay People's Trust Council* (MARA) and Universiti Putra Malaysia.

References

[1] McVicar JSG (1993), *A Generic Tilt-Rotor Simulation Model with Parallel Implementation*. University of Glasgow
[2] Renaud JP (2000), Advanced technologies and new roles for VTOL aircraft: Part I. *Air & Space Europe* 2(2)
[3] DeTore J & Conway S (1991), Technology needs for high speed rotorcraft. National Aeronautics and Space Administration
[4] Bell (1969), *Advancement of proprotor technology: Task 1-Design Study Summary*. Fort Worth, TX
[5] Smith RD (1996), Civil tiltrotor - A new transportation alternative. World Aviation Congress
[6] Wernicke KG (1969), Tilt proprotor composite aircraft, design state of the art. *J. Am. Helicopter Soc.* 14(2), 10-25
[7] Anon (1991), Civil tiltrotor missions and applications-Phase II: The commercial passenger market. National Aeronautics and Space Administration and Federal Aviation Administration
[8] Dreier ME (2007), Introduction to helicopter and tiltrotor flight simulation. American Institute of Aeronautics and Astronautics
[9] Padfield GD (2007), *Helicopter Flight Dynamics: The Theory and Application of Flying Qualities and Simulation Modelling*. Oxford, UK: Blackwell Publishing Ltd
[10] Johnson W & Sinsay JD (2009), Rotorcraft conceptual design environment. 3rd International Basic Research Conference on Rotorcraft Technology
[11] Johnson W & Datta A (2008), Requirements for next generation comprehensive analysis of rotorcraft. AHS Specialist's Conference on Aeromechanics
[12] Russell C & Johnson W (2013), Application of climate impact metrics to civil tiltrotor design. 51st AIAA Aerospace Sciences Meeting
[13] Filippone A (2006), *Flight Performance of Fixed and Rotary Wing Aircraft*. Burlington, MA: Butterworth-Heinemann
[14] Newman S (1994), *The Foundations of Helicopter Flight*. London, UK: Butterworth-Heinemann
[15] Goulos I (2012), *Simulation Framework Development for the Multidisciplinary Optimisation of Rotorcraft*. Cranfield University
[16] Harendra PB, Joglekar MJ, Gaffey TM & Marr RL (1973), *V/STOL Tilt Rotor Study - Volume V: A Mathematical Model For Real Time Flight Simulation of the Bell Model 301 Tilt Rotor Research Aircraft*. Fort Worth, Texas
[17] Ferguson SW (1988), A mathematical model for real time flight simulation of a generic tilt-rotor aircraft. National Aeronautics and Space Administration

[18] Gires E (2016), *Preliminary Design and Performance Optimisation of Advanced Powerplants for Tiltrotor Aircraft.* Cranfield University
[19] Hanson GD & Ferguson SW (1988), *Generic Tilt-Rotor Simulation (GTRSIM) User's and Programmer's Guide*. Moffett Field, CA
[20] Johnson W (2010), NDARC — NASA design and analysis of rotorcraft validation and demonstration. American Helicopter Society Aeromechanics Specialists' Conference
[21] Johnson W (2010), NDARC — NASA design and analysis of rotorcraft theoretical basis and architecture. National Aeronautics and Space Administration
[22] Nikolaidis T (2015), *The Turbomatch Scheme - For aero/ Industrial Gas Turbine Engine Design Point/ Off Design & Transient Performance Calculation*. Cranfield University
[23] Jane's (2012), Jane's Aero Engines. Jane's Information Group, IHS
[24] Rubins PM & Doyle BW (1973), T53 and T55 gas turbine combustor and engine exhaust emission measurements. Army Air Mobility Research and Development Laboratory
[25] Dugan DC, Erhart RG & Schroers LG (1980), The XV-15 tilt rotor research aircraft. National Aeronautics and Space Administration
[26] Rindlisbacher T (2009), Guidance on the determination of helicopter emissions. Federal Office of Civil Aviation
[27] Ali F (2014), *Design and Optimisation of Rotorcraft Powerplants*. Cranfield University
[28] Zhang J (2014), *Coaxial Rotorcraft Power-plant Simulation and Optimisation*. Cranfield University
[29] Churchill GB & Dugan DC (1982), Simulation of the XV-15 tilt rotor research aircraft. National Aeronautics and Space Administration
[30] Johnson W (2010), NDARC — NASA design and analysis of rotorcraft validation and demonstration. National Aeronautics and Space Administration
[31] Ferguson SW (1989), Development and validation of a simulation for a generic tilt-rotor aircraft. National Aeronautics and Space Administration
[32] Wernicke K & Magee J (1979), XV-15 flight test results compared with design goals. AIAA Aircraft Systems and Technology Meeting
[33] NASA (1975), NASA/Army XV-15 tilt rotor research aircraft familiarization document. National Aeronautics and Space Administration
[34] Raisbeck (2009), *FAA-Approved Pilot's Operating Handbook and Airplane Flight Manual Supplement for the Beechcraft Super King Air Models 200/200C/B200/B200C*. Raisbeck Engineering
[35] Conner DA, Marcolini MA, Decker WA, Cline JH, Edwards BD, Nicks CO & Klein PD (1999), XV-15 tiltrotor low noise approach operations. American Helicopter Society 55th Annual Forum
[36] Bianco-Mengotti R (2012), The AgustaWestland path to the new generation tilt-rotor: Technological challenges for the future of rotary wing. http://www.aofs.org/wp-content/uploads/2012/11/121122.11-AW-path-to-new-generation-tiltrotor1.pdf.